17th World Conference on Earthquake Engineering, 17WCEE
Sendai, Japan - September 13th to 18th 2020

Coupled Axial Tension-Shear Behavior of Reinforced Concrete Walls

X. Ji[(1)], X. Cheng[(2)], M. Xu[(3)]

[(1)] *Associate professor, Department of Civil Engineering, Tsinghua University, jixd@mail.tsinghua.edu.cn*
[(2)] *Ph.D. student, Department of Civil Engineering, Tsinghua University, cxw15@mails.tsinghua.edu.cn*
[(3)] *Graduate student, Department of Civil Engineering, Tsinghua University, xumc16@mails.tsinghua.edu.cn*

Abstract

Reinforced concrete (RC) shear walls in a high-rise building may experience coupled axial tension-shear loading when subjected to strong ground motions. In such a case, axial tensile forces may significantly influence the shear strength and stiffness of RC walls, leading to force redistribution among structural components. To understand how the tensile force influences shear behavior of RC walls, a series of quasi-static tests were conducted on six low-aspect-ratio wall specimens. The wall specimens were subjected to combined axial tensile forces and cyclic shear loading. Although all specimens had identical geometry and reinforcement, their failure modes varied with different magnitudes of axial tensile force. These failure modes included diagonal tension failure (no axial tensile force), shear-sliding failure (normalized concrete tensile tress n_c = 0.51 - 1.43) and sliding failure (n_c = 2.26 - 2.79). The shear strength of RC wall specimens decreased linearly with increasing axial tensile force, with a factor of approximately 0.35. Sliding shear strength of specimens subjected to high axial tensile force was only 24% - 33% of the shear strength capacity of the specimen having no axial load. High axial tensile force also resulted in a significant decrease in lateral stiffness of the walls. Finally, design formulae of shear stiffness and strength of RC walls under axial tension were estimated by comparison with test data. The strut-and-tie model provided a reasonable estimate of effective lateral stiffness of low-aspect-ratio RC walls under low to moderate tensile force. The design formulae specified in ACI 318-14 (U.S.) code provided a conservative estimate of the shear strength capacity of the RC walls subjected to tensile forces. The average experimental-to-calculated ratio was 1.68. However, the JGJ 3-2010 formulae (China) tended to overestimate the shear strength capacity under moderate axial tensile forces.

Keywords: RC shear walls, coupled axial tension-shear behavior, design formulae, shear strength, shear stiffness

1. Introduction

Reinforced concrete (RC) walls are widely used as the major lateral load-resisting components in high-rise buildings. When subjected to strong ground motions, some structural walls, in particular wall piers that form part of a coupled or core wall system, may experience combined axial tension-shear load. For example, in a coupled wall system with a high coupling ratio the axial forces induced by coupling beam shears may result in the wall pier sustaining a net axial tensile force, combined with shear force induced by lateral loading, as illustrated in Fig. 1(a). Another example is a core wall under bi-directional ground motion, as shown in Fig. 1(b), where the peripheral wall is subjected to the tensile force caused by a large overturning moment from lateral loading in one direction, and the shear force induced by lateral loading in the perpendicular direction. Past earthquake reconnaissance (e.g., the 2010 Chile earthquake [1]), and experimental tests of coupled and core wall systems (e.g., [2-5]) identified such critical loading conditions for RC walls in high-rise buildings.

Past research indicates that axial tension leads to decreased stiffness and strength of RC walls, and may results in lateral force redistribution among structural components [2-5]. Therefore, special attention shall be given to RC walls that may be subjected to combined axial tension-shear load during seismic design of high-rise buildings. However, fundamental experimental research on coupled axial tension-shear behavior of RC walls remains very limited.

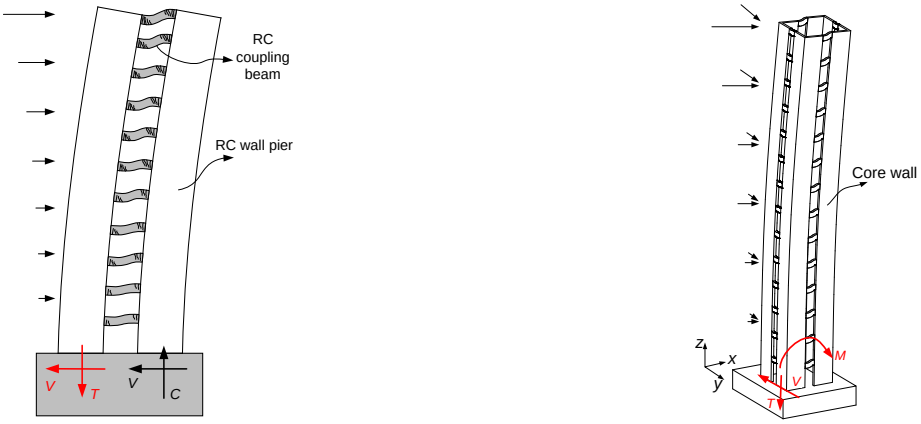

(a) Coupled wall (b) Core wall

Fig. 1 – RC walls undergoing coupled axial tension-shear forces

More recently, effort has been devoted to the study of coupled tensile-shear behavior of RC walls. Wang et al. [6] conducted experimental tests of five RC wall specimens with a shear-to-span ratio of 1.45, where the specimens were subjected to the axial tensile forces and cyclic shear loading. Heavy boundary longitudinal reinforcement, corresponding to a 10.9% reinforcement ratio of the boundary elements, were intentionally used to ensure that flexural strength of the wall specimens exceeded their shear strength. These wall specimens failed in a shear failure mode. The wall's shear strength and stiffness was found to significantly decrease with an increase of axial tensile forces.

The objective of this study is to determine how axial tensile forces influence failure mode and the shear strength and stiffness of RC walls with low shear-to-span ratio. An experimental program is presented that involves six wall specimens subjected to tensile forces and cyclic shear loading. The test results are detailed in terms of failure mode, hysteretic response, and shear strength and deformation capacities. Finally, estimates of relevant design formulae of the shear stiffness and strength of RC walls under tensile forces are presented in comparison with test data.

2. Experimental program

2.1 Test specimens

Test specimens were designed to represent RC walls in the lower story of a high-rise building and were fabricated at approximately one-third-scale to accommodate the capacity of loading facility. The shear-to-span ratio of the walls varies in different situation and loading cases, which is influenced by the structural layout, high mode effect, and ground motions, etc. The experimental tests for RC walls with a high shear-to-span ratio are reported in [7]. This paper presents the experimental tests of RC walls with a relatively low shear-to-span ratio of 1.1. A total of six shear wall specimens (SW1 to SW6) were designed and fabricated, each with identical dimensions and reinforcement details. As shown in Fig. 2, the clear height of wall specimens above the foundation was 1.35 m, with a sectional depth and thickness of 1.5 m and 0.18 m, respectively. The foundation and top beams were intentionally designed with large dimensions and heavy reinforcement to ensure they remained damage-free during testing. The foundation beams were fabricated first, followed by construction of the wall and top beams. The surface of the hardened concrete of the foundation beam was carefully roughened before casting of the wall concrete to mitigate the adverse influence of construction joints.

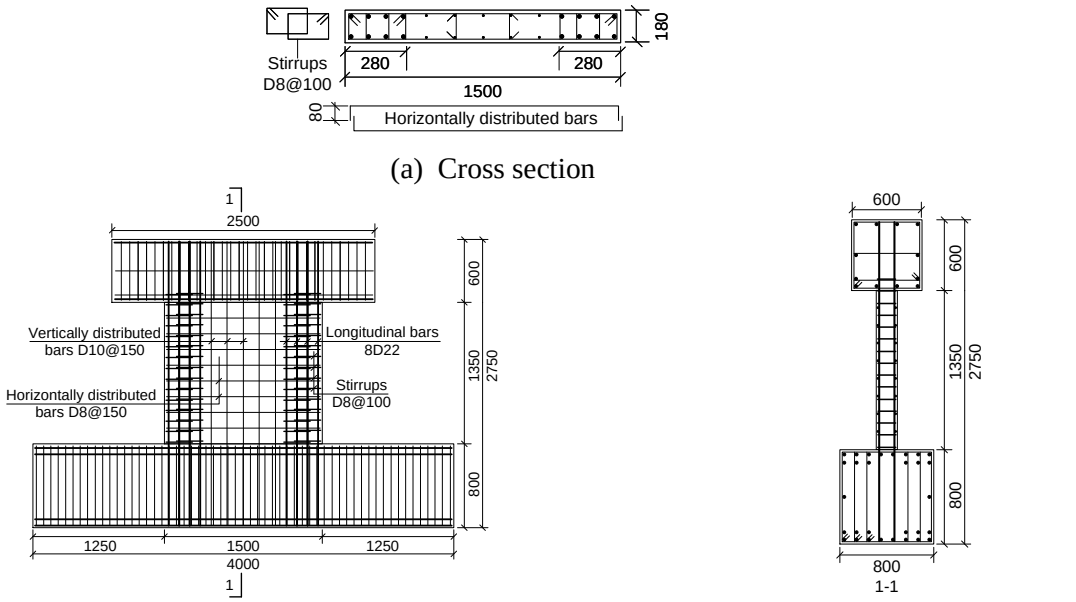

(a) Cross section

(b) Elevation view

(c) Elevation view 1-1

Fig. 2 – Geometry and reinforcement of specimens (units: mm)

Eight D22 (diameter of 22 mm) steel reinforcing bars (hereinafter referred to as rebar) were used as boundary longitudinal reinforcement for all specimens, corresponding to a 5.6% reinforcement ratio of the boundary element. The high reinforcement ratio was intended to ensure that flexural strength of the wall specimens exceeded their shear strength capacity.

D10 steel rebar was used as vertically distributed reinforcement in the web of the specimens at a spacing of 150 mm, which corresponds to a 0.58% reinforcement ratio. D8 steel rebar was used as horizontally distributed reinforcement at a spacing of 150 mm, corresponding to a 0.37% reinforcement ratio. The boundary transverse reinforcement consisted of D8 steel rebar fabricated as rectangular hoops with a vertical spacing of 100 mm (1.5% volumetric transverse reinforcement ratio). The boundary elements and reinforcement of the specimens satisfies the requirement of seismic ductile walls specified in the Chinese Technical Specification for Concrete Structures for Tall Buildings (JGJ 3-2010) [8].

The strength grade of concrete used in the wall specimens was C55 (nominal cubic compressive strength $f_{cu,n}$ = 55 MPa). The measured compressive strength f_{cu} of the concrete using the 150 mm cubes was 62.9, 63.4, 63.6, 56.7, 58.1 and 55.4 MPa for specimens SW1 through SW6. The value of f_{cu} was measured on the day of specimen testing, and it was taken as the average value for three cubes. The axial compressive strength of concrete f_c was taken as $0.76f_{cu}$ in accordance with the Chinese Code for Design of Concrete

Structures GB 50010-2010 [9]. The assumed value of axial tensile strength of concrete (f_t) was taken as $0.395 f_{cu}^{0.55}$ in accordance with GB50010-2010 [9].

All steel rebar used for the wall specimens had a strength grade HRB400 (nominal yield strength $f_{y,n}$ = 400 MPa). Table 1 summarizes the measured reinforcement yield strength, ultimate strength and uniform elongation (i.e., measured strain corresponding to the peak stress). These are the average values obtained by three standard rebar tensile tests for each type of steel rebar.

Table 1 – Material properties of steel rebar used in experimental specimens

Spec. no.	Diameter (mm)	Yield strength f_y (MPa)	Ultimate strength f_u (MPa)	Uniform elongation δ (%)
SW1 through SW3	8	397.9	671.2	11.4
	10	396.3	633.9	19.8
	22	349.0	530.9	18.8
SW4 through SW6	8	480.0	740.0	10.8
	10	465.0	721.7	16.2
	22	478.3	653.3	20.7

2.2 Axial tensile force

Two indices are defined to quantify the magnitude of axial tensile force [6, 7]. They are the normalized concrete tensile stress (n_c) and normalized reinforcement tensile stress (n_s), as shown below:

$$n_c = \frac{T_n}{\left(A_c + A_s E_s / E_c\right) f_t} \tag{1}$$

$$n_s = \frac{T_n}{A_s f_y} \tag{2}$$

where T_n denotes the axial tensile force of the wall, A_c denotes the cross-sectional area of concrete, A_s denotes the cross-sectional area of vertical reinforcement (including vertically distributed rebar and boundary longitudinal rebar), E_s and E_c denote the elastic modulus of steel and concrete, respectively, and f_y and f_t denote the tensile yield strength of steel and axial tensile strength of concrete, respectively.

For $n_c \leq 1$, the value of n_c represents the ratio of nominal axial tensile stress to concrete tensile strength. However, for $n_c > 1$, concrete sustains tensile cracking and the tensile force is carried only by vertical reinforcement at the cracked sections. In this situation, the value of n_s reflects the degree of tensile force and $n_s = 1$ corresponds to the axial tensile yield strength of RC walls.

Table 2 summarizes the values of axial tensile force and the values of n_c and n_s for the six specimens. In the calculation, the measured strengths of concrete and rebar were adopted. As n_c is commonly used in practical design in China, it is used to quantify the axial tensile force values in the following discussion. Specimens SW1 and SW2 were subjected to low tensile forces ($n_c < 1.0$). Specimen SW3 was subjected to moderate tensile force ($1.0 < n_c < 2.0$). Specimens SW4 and SW5 were subjected to high tensile forces ($n_c > 2.0$) and no axial tensile force was applied to SW6.

Table 2 – Axial tensile force values of RC wall specimens

Spec. no.	SW1	SW2	SW3	SW4	SW5	SW6
T_n / (kN)	617	1030	1716	2553	3192	0
n_c	0.51	0.86	1.43	2.26	2.79	0
n_s	0.23	0.38	0.63	0.80	1.00	0

2.3 Test setup and instrumentation

The test setup is shown in Fig. 3. The foundation beam was clamped to the reaction floor and the top beam was clamped to three hydraulic actuators, one in the horizontal direction and two in the vertical direction. Out-of-plane support was provided to prevent out-of-plane deflections and twisting of the wall specimen during testing.

Two phases of loading were included in testing. The first phase consisted of applying the vertical axial tension to the specimen using the vertical actuators with increments of $0.2T_n$ until the target tensile force T_n was reached. Afterwards, the vertical tensile force was maintained constantly. The second phase of loading consistes of the cyclic shear loads that were applied by the horizontal actuator. The centroid of the horizontal actuator was located 1650 mm above the wall base, resulting in a shear-to-span ratio of the wall of 1.1.

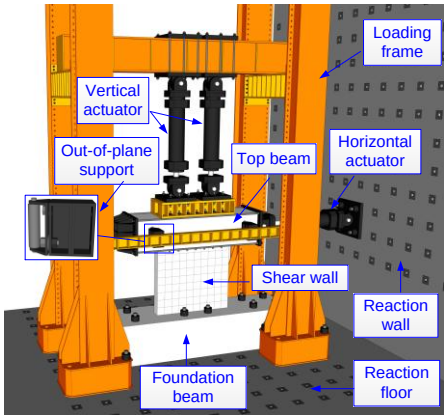

Fig. 3 – Test setup

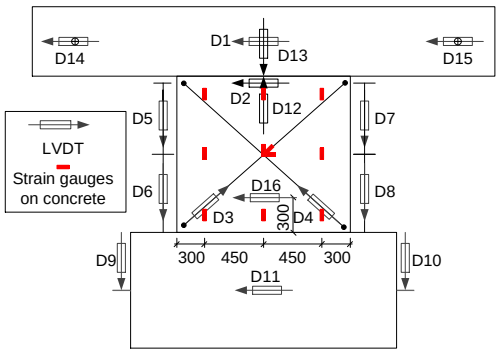

Fig. 4 – Layout of instruments

The history of cyclic shear loading was determined based on the Chinese Specification for Seismic Testing of Buildings (JGJ 101-2015) [10]. In the elastic region, two levels of lateral drift loading were included (0.1% and 0.2%) and one cycle was performed at each level. After the specimen reached the predicted yield drift (i.e., 0.35%), the lateral displacement load was increased at 0.25% increments, and two cycles were repeated at each drift level. The test was terminated when the lateral force of the specimen dropped below 85% of the maximum lateral force or the specimen could not sustain the tensile force due to fracture of the vertical reinforcement.

It is acknowledged that cyclic loading in this testing scheme, combined with initially applied constant axial tensile forces and increased cyclic shear forces, may not exactly represent the actual loading condition of walls in a high-rise building. When subjected to ground motion, axial tensile forces in the walls vary as well. Nevertheless, the loading method in this program provides an effective way to examine how different magnitudes of axial tension affect shear behavior of the walls, which is the objective of the study. The effect of loading history is left for future study.

Values of load, displacement and strain were measured for each specimen. Load cells were used to measure vertical tension and lateral shear forces. The layout of linear variable differential transformers (LVDTs) mounted on the specimen is shown in Fig. 4. The LVDTs measured the lateral displacement, shear deformation, flexural deformation, and axial elongation of the wall. Eight strain gauges and a set of strain gauge rosettes were mounted on the wall (Fig. 4) to measure strain in the wall concrete. A further 29 strain gauges were mounted on the distributed rebar, as well as on the boundary longitudinal and transverse rebar.

3. Experimental results

3.1 Damage and failure modes

In the first phase of loading (axial tensile loading), horizontal tensile cracks were observed in the wall specimens. In the second phase of loading (cyclic shear loading), the damage was fully developed.

Photographs of the specimens after testing (Fig. 5) demonstrate three types of failure modes: (a) diagonal tension failure (SW6); (b) shear-sliding failure (SW1, SW2 and SW3) and (c) sliding failure (SW4, SW5).

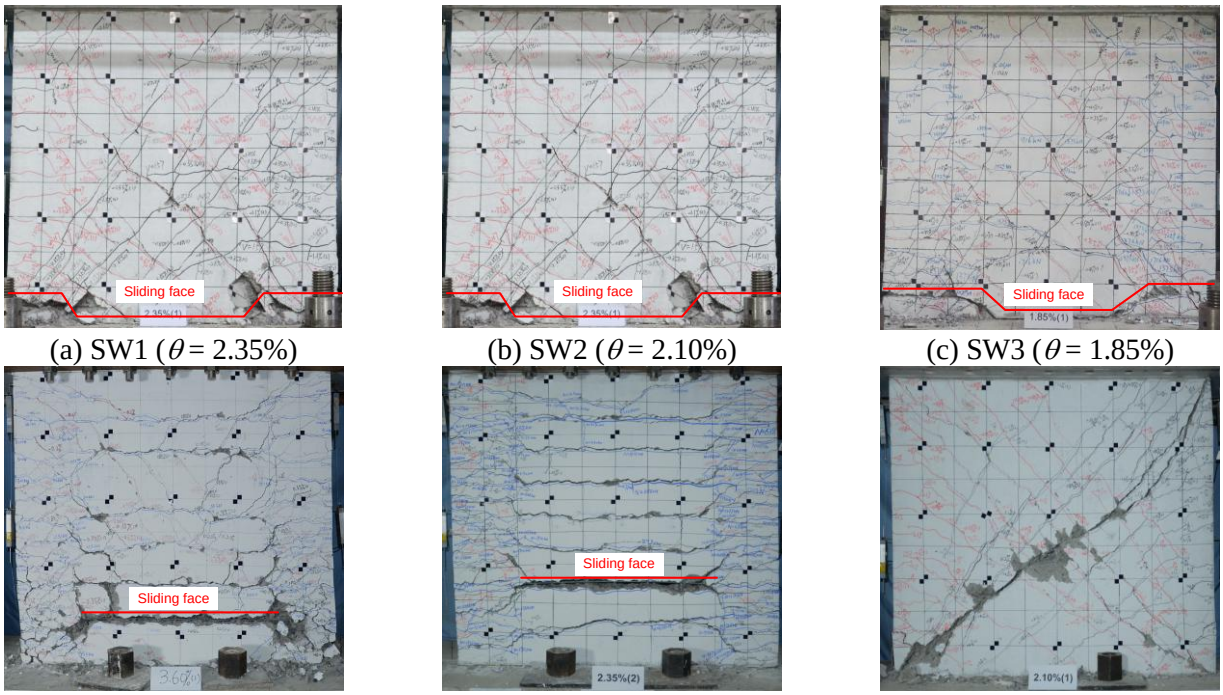

(a) SW1 (θ = 2.35%) (b) SW2 (θ = 2.10%) (c) SW3 (θ = 1.85%)

(d) SW4 (θ = 3.6%) (e) SW5 (θ = 2.35%) (f) SW6 (θ = 2.1%)

Fig. 5 – Photographs of specimens after testing

Diagonal tension failure: Specimen SW6, having no axial load, sustained diagonal tension failure. At 0.1% drift, inclined cracks occurred in the wall web and a number of horizontal cracks were observed at the wall boundary. With increased cyclic shear loading, inclined and crisscrossed cracks continued to develop. A major diagonal crack developed fully at the peak load (0.85% drift), as shown in Fig. 5(f). Upon further loading, sliding occurred along the diagonal failure plane. At 1.35% drift, another diagonal failure plane, perpendicular to the existing failure plane, was observed. Thus, the two failure planes divided the wall into four blocks. The rebar that passed through the diagonal failure planes buckled and kinked when the blocks slid along the failure planes. At 1.6% drift, the concrete cover spalled along the diagonal failure planes. Loading terminated at 2.1% drift when the shear strength decreased below 85% of the lateral peak load.

Shear-sliding failure: Specimens SW1, SW2 and SW3, having low to moderate axial tensile load, sustained shear-sliding failure characterized by full development of shear strength of the wall and transition into sliding failure along the wall base. At 0.35% drift, inclined cracks became evident in the wall web. Upon further loading, there was significant development of crisscrossed diagonal cracks. At 0.85% drift, the wall specimens reached the peak lateral load, and at 1.1% drift, a horizontal sliding surface formed at the wall base (Fig. 5(a) to (c)). The wall slid noticeably along this plane, particularly when subjected to positive loading. The horizontal sliding surface developed along the construction joints between the wall web and foundation beam. The sliding surface bent upwards at the wall boundary elements because the high ratio of boundary longitudinal rebar prevented sliding of the boundary element along the wall-to-foundation beam interface. Meanwhile, a pair of major corner-to-corner diagonal crack formed with slight sliding observed.

The mechanism of shear-sliding failure, where shear behavior shifts to sliding failure, is illustrated in Fig. 6. Shear behavior in the wall specimens was dominated during small lateral loadings, and was characterized by development of inclined cracks (Fig. 6(a)). It is evident that the bending moment increased at the wall base as shear forces increased and horizontal cracks developed due to combined axial tensile force and bending moment (Fig. 6(b)). Under cyclic reversal, flexural horizontal cracks extended from both edges and finally developed into a continuous, approximately horizontal, sliding surface (Fig. 6(c)).

The total sliding shear resistance was developed by both the shear-friction mechanism at the compressive zone where the base cracks closed upon a load reversal and the doweling action of vertical rebars. After the boundary longitudinal rebars yielded, the opening of the flexural crack widened with increased lateral drift. The compression zone became smaller, resulting in a decrease in the sliding shear resistance along the sliding surface. When sliding shear resistance decreased below the shear strength, sliding occurred and there was a shift to sliding-dominated behavior (Fig. 6(d)).

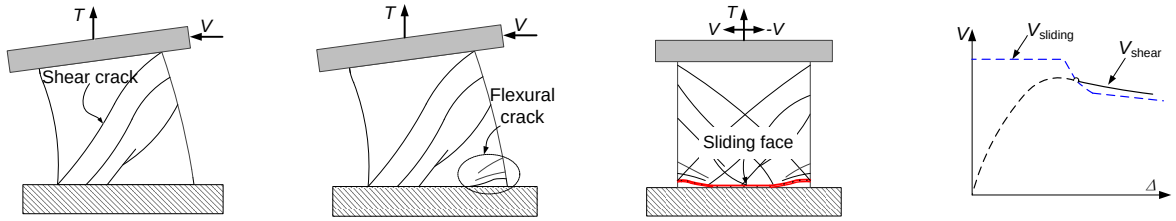

Fig. 6 – Schematic diagrams illustrating the mechanism of shear-sliding failure

Sliding failure: Specimens SW4 and SW5, having high axial tensile load, underwent sliding failure. After applying axial tensile force, several continuous horizontal cracks developed along the height of the wall. At 0.85% drift, the widest horizontal crack induced by the initial tensile loading developed to form a critical sliding face. At 1.35% drift, significant sliding deformation occurred along the sliding face. At 2.35% drift, the critical sliding crack width reached 15 mm, and the vertically distributed rebar kinked at the sliding face. Ultimately, SW4 failed because of crushed concrete at the corners of the walls, whereas SW5 failed because the vertically distributed rebar fractured.

3.2 Hysteretic response

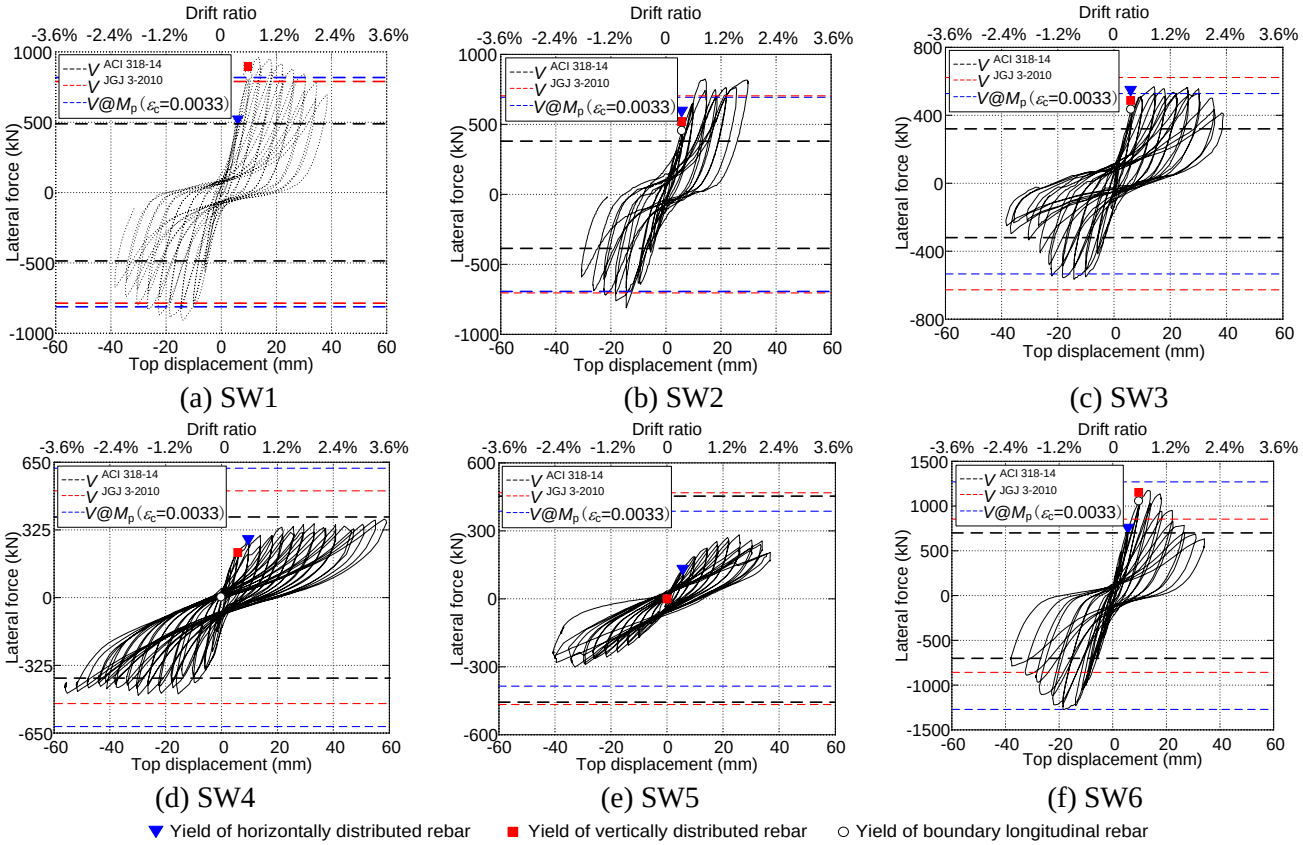

Fig. 7 – Hysteretic loops of lateral force versus top displacement for specimens

Hysteresis curves of lateral force versus top lateral displacement for six specimens are shown in Fig. 7. The points corresponding to the yielding of horizontally distributed rebar, vertically distributed rebar and boundary longitudinal rebar are identified in this figure, which were determined based on strain gauge data.

Three main observations are made from Fig. 7: (1) SW1 and SW6 showed rapid post-peak strength degradation compared with other specimens. Although SW1 failed in a shear-sliding failure mode, its hysteretic loop was similar to that of SW6, as its sliding deformation was relatively small and the total drift was dominated by shear deformation. The horizontally distributed rebar yielded prior to both the vertically distributed and boundary longitudinal rebar. (2) The post-peak strength of SW2 and SW3 remained stable during positive loading while it decreased significantly during negative loading. This is attributed to the fact that sliding along the horizontal sliding surface mainly occured during positive loading, while drift in the negative direction was dominated by shear deformation. The horizontally and vertically distributed rebar, and the boundary longitudinal rebar, all yielded at the same drift of 0.35%. (3) The post-peak strength of SW4 and SW5, which failed by sliding, remained very stable even under large drift. Specimen SW5 had a smaller ultimate displacement than SW4 because of tensile fracture of the vertically distributed rebar. For sliding failure, it is evident that the vertically distributed rebar and boundary longitudinal rebar yields prior to the horizontally distributed rebar.

3.3 Shear strength and deformation capacities

Table 3 presents the values of measured yield load (V_y) and corresponding yield drift (Δ_y), the peak load (V_p) and corresponding drift (Δ_p), and the ultimate drift (Δ_u) and corresponding drift ratio (θ_u). The measured yield point is determined using the idealized force-displacement curve method in accordance with ASCE/ SEI 41-13 [11]. Ultimate drift is defined as the post-peak drift at the instant when the lateral load decreases to 85% of the peak load. For SW4, the post-peak strength did not decrease below 85% of the peak load until complete failure. In such a case, the ultimate displacement is defined as the maximum drift that the specimen endures with a full cycle before complete failure. The values shown in Table 3 are the average values measured during positive and negative loading.

Values in Table 3 indicate that axial tensile forces significantly influence the lateral load-carrying capacity of the wall specimens. The shear strengths of SW1, SW2, SW3 and SW6 decreased markedly along with increasing axial tensile force. For SW4 and SW5, which were subjected to high axial tensile force and were governed by sliding failure, the maximum sliding shear strengths were lower by 67% and 76% than the shear strength of SW6 that had no axial load. The ultimate drift ratio of SW1 to SW5, which failed in shear-sliding or sliding modes were larger than in SW6, which failed in a diagonal tension mode, because sliding along the cracks increased the lateral drift capacity.

Table 3 – Lateral strength and deformation capacities of specimens

Spec. no	Δ_y/mm	V_y/kN	Δ_p/mm	V_p/kN	Δ_u/mm	θ_u
SW1	9.8	883.0	13.8	934.0	32.1	1.9%
SW2	7.5	588.5	14.3	817.4	27.9	1.7%
SW3	5.6	458.8	14.2	567.3	29.7	1.8%
SW4	4.5	281.5	21.6	398.5	56.7	3.4%
SW5	7.9	175.8	29.3	291.8	37.2	2.3%
SW6	7.6	877.2	15.7	1224.6	24.1	1.5%

4. Evaluation of lateral stiffness and shear strength

4.1 Lateral stiffness

The initial elastic lateral stiffness of RC walls, taking both flexural and shear deformation into consideration can be calculated as follows:

$$K_0 = 1/\left(\frac{H^3}{3EI} + \frac{kH}{GA}\right) \tag{3}$$

where K_0 denotes the initial elastic lateral stiffness, H denotes wall height, EI denotes the flexural stiffness of a wall section, GA denotes the shear stiffness of wall section and k is the form factor accounting for nonuniform shear stresses across the section depth, which is taken as 1.2 for rectangular sections [12].

After concrete cracking, the effective flexural stiffness $(EI)_{cr}$ is specified at a value of $0.35EI$ by the ACI 318-14 code for cracked RC walls [13]. Moehle [12] recommends a simplified method for calculating shear stiffness of cracked RC walls based on truss idealization (strut-and-tie model). In such a model, shear deformation is assumed to be induced by shortening of the diagonal compressive concrete struts and elongation of the transverse reinforcement ties. In accordance with this method, the shear stiffness $(GA)_{cr}$ of cracked RC walls can be calculated as follows:

$$(GA)_{cr} = \frac{n\rho_h \cos^2\theta_c \sin^2\theta_c}{0.4(\cos^4\theta_c + \rho_h n)} G_c A_w \tag{4}$$

where $(GA)_{cr}$ denotes the shear stiffness of cracked RC walls, $n = E_s/E_c$ denotes the ratio of elastic modulus of steel to that of concrete, ρ_h denotes the reinforcement ratio of horizontally distributed rebar, θ_c denotes the inclination angle of inclined cracks, which is taken as 45 ° in this calculation, A_w denotes the cross-sectional area of web.

Using $(EI)_{cr}$ and $(GA)_{cr}$ instead of EI and GA in Eq. (3), the effective lateral stiffness K_{eff}^{Cal} of RC walls can be calculated. Fig. 8 shows a comparison between K_{eff}^{Cal} and the test values (K_{eff}^{Test}) of the wall specimens (i.e., the secant stiffness at the measured yield point). The following observations are made from Fig. 8: (1) The value of K_{eff}^{Cal} is approximately 10% of the initial elastic lateral stiffness (K_0) for the low-aspect-ratio wall specimens. (2) The estimated value of K_{eff}^{Cal} correlates well with the measured value of K_{eff}^{Test} for SW1, SW2 and SW3 that had low to moderate tension forces. (3) For SW4 and SW5, with high axial tensile forces, the values of K_{eff}^{Test} are lower than the calculated values because the strut-and-tie model does not include horizontal sliding displacement. (4) Very high axial tension would significantly decrease the effective lateral stiffness of the wall. For SW5 (n_c = 2.79), the value of K_{eff}^{Test} was only 20% of that of SW6. In structural design, special attention needs to be given to the significant lateral stiffness decrease for RC walls subjected to high axial tensile forces.

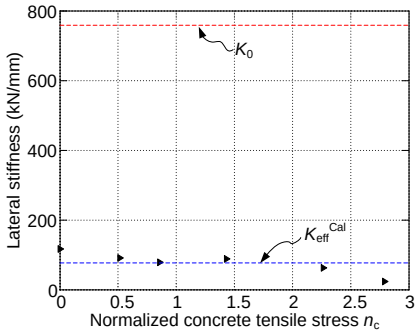

Fig. 8 – Lateral stiffness of specimens

4.2 Shear strength design formulae for RC walls under tension

Table 4 presents the ACI 318-14 (U.S.) [13] and JGJ 3-2010 (China) [8] code formulae for calculating shear strength of RC walls subjected to axial tensile forces. In these design formulae, the total shear strength of RC walls is calculated by superposition of the shear contribution of the concrete (V_c) and the shear contribution of the horizontally distributed rebar (V_s). The value of V_c depends on the shear-to-span ratio and axial forces. The factor related to axial tensile force is different in the formulae of two codes. A value of 0.13 is taken for code JGJ 3-2010 and a value of 0.20 in code ACI 318-14.

Table 4 – Design formulae for shear strength of RC walls under tensile force.

JGJ 3-2010 (China)	$V=\frac{1}{\lambda-0.5}\left(0.5f_{t}b_{w}h_{w0}-0.13T\right)+f_{yh}\frac{A_{sh}}{s}h_{w0}$ If λ<1.5, λ=1.5	(5)
ACI 318-14 (U.S.)	$V_1=0.27\sqrt{f_c'}b_{w}h_{w0}-\frac{Th_{w0}}{4h_{w}}+f_{yh}\frac{A_{sh}}{s}h_{w0}$	(6)
	$V_2=(0.05\sqrt{f_c'}+\frac{1}{\lambda\text{-}0.5}(0.1\sqrt{f_c'}-\frac{0.2T}{h_{w}b_{w}}))b_{w}h_{w0}+f_{yh}\frac{A_{sh}}{s}h_{w0}$	(7)
	$V=\min(V_1,V_2)$ h_{w0}> $0.8h_{w}$	(8)

It should be noted that V denotes the shear strength of the RC wall under axial tension, f_c' denotes the compressive strength of concrete in MPa, h_w denotes the sectional depth of the wall, b_w denotes the wall thickness and h_{w0} denotes the effective sectional depth of the wall, T denotes the axial tension force applied to the wall, f_{yh} denotes the yield strength of horizontally distributed rebar, s denotes the vertical spacing of horizontally distributed rebar, A_{sh} denotes the area of horizontally distributed rebar within the spacing s, and $\lambda = Mh_{w0}/V$ denotes the shear-to-span ratio of the wall.

4.3. Validation of design formulae

Using the data from this program and past tests, the section estimates the design formulae of shear strength of RC walls subjected to tensile forces. Wang [6] conducted quasi-static tests on four RC shear walls (SW-1 through SW-4) subjected to axial tensile forces and cyclic shear loading. All wall specimens had identical geometric dimensions and reinforcement, as shown in Fig. 9. The walls had a rectangular-shaped section with an overall sectional depth of 1000 mm and wall thickness of 120 mm.

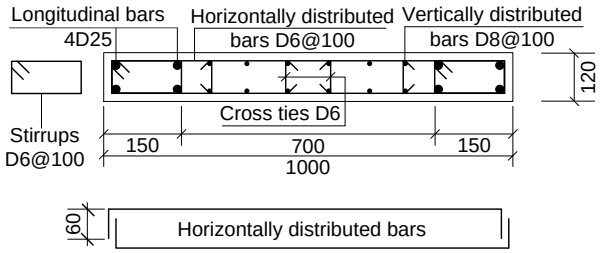

Fig. 9– Cross sectional dimensions and reinforcement of wall specimens in Wang et al. [6] (units: mm)

The wall specimens were loaded as a cantilever, with a moderate shear-to-span ratio of 1.45. The wall had a reinforcement ratio of 0.48% for horizontally distributed rebar and 0.72% for vertically distributed rebar. The measured yield strength values of steel (f_y) were 445, 582 and 661 MPa for D25, D8 and D6 rebar, respectively. The measured cubic compressive strength of concrete (f_{cu}) was 46.9 MPa. The applied values of axial tensile force were 0, 176, 380 and 578 kN for SW-1, SW-2, SW-3 and SW-4, respectively. These values correspond to n_c values of 0, 0.38, 0.79 and 1.20, respectively. Specimen SW-1 failed by diagonal tension failure characterized by a major diagonal failure plane. Specimens SW-2, SW-3 and SW-4 failed in shear characterized by extensive crisscrossed inclined cracks in the wall web.

Table 5 compares the estimated shear strength values obtained from design formulae with the maximum shear strength values measured in the tests. Given that SW4 and SW5 failed by sliding before fully developing their shear strength, they are not included in the comparison. Table 5 indicates that the ACI 318-14 code formulae provide a conservative estimate of the shear strength capacity. The mean value of the V^{Test}/V^{ACI} ratio is 1.68 (standard deviation of 0.26). Although the mean value from the JGJ 3-2010 code formulae provides a V^{Test}/V^{JGJ} ratio of 1.10 for all specimens, it overestimates the shear strength for the specimens subjected to moderate tensile forces ($1.0 < n_c < 2.0$), with an average experimental-to-calculated ratio of 0.93. Considering the nature of brittle shear failure, conservative estimates of shear strength are

preferable in design. Therefore, an adjustment to the JGJ 3-2010 formula appears necessary. It is interesting to note that the estimates of specimens in this study (shear-to-span ratio λ = 1.1) and those of Wang (λ = 1.45) have different degrees of safety redundancy. The mean value of the V^{Test}/V^{ACI} ratio is 1.90 for the former specimens and 1.45 for the latter specimens. It is left for future study on the effect of the shear-to-span ratio.

Table 5 – Comparison between measured and estimated strengths

	Spec. no	n_c	V^{Test} (kN)	V^{JGJ} (kN)	V^{ACI} (kN)	V^{Test}/V^{JGJ}	V^{Test}/V^{ACI}
This paper	SW1	0.51	934.0	749.4	488.0	1.25	1.91
	SW2	0.86	817.4	695.2	378.2	1.17	2.16
	SW3	1.43	567.3	606.6	319.5	0.93	1.77
	SW6	0	1224.6	871.2	697.9	1.40	1.75
Wang et al.	SW-1	0	603.0	528.1	390.6	1.14	1.54
	SW-2	0.37	543.0	505.2	361.0	1.07	1.50
	SW-3	0.79	436.0	478.7	326.6	0.91	1.33
	SW-4	1.20	427.0	453.0	299.3	0.94	1.43
					Mean	1.10	1.68
					Standard deviation	0.16	0.26

Additional analysis is used to quantify the influence of axial tensile force on the shear strength capacity of RC walls. The relationship between the normalized shear strength of the concrete and the normalized axial tensile stress of the concrete is plotted in Fig. 10 (note that the shear force carried by the reinforcement has been removed in the calculation of normalized concrete shear strength). The concrete shear strength appears to decrease linearly as axial tensile stress increases, with a factor of approximately 0.35. The JGJ 3-2010 and ACI 318-14 code formulae are also plotted in Fig. 10.

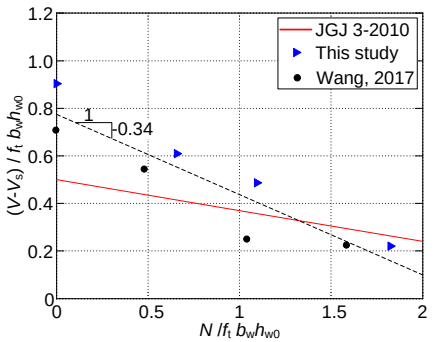

(a) JGJ 3-2010

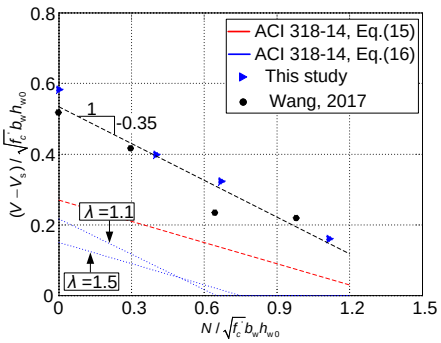

(b) ACI 318-14

Fig. 10 – Measured and calculated shear strengths based on U.S. and Chinese design formulae

The JGJ code formula overestimates the shear strength of RC shear walls when n_c>1.0 because the factor of axial tensile force specified (0.13) is significantly lower than 0.35. The ACI 318-14 code formulae produce a conservative estimate of the shear strength of RC walls under a wide range of tensile force values. However, the safety redundancy for this estimate varies for different values of tensile force, and more data is needed for improved calibration and adjustment of the formulae.

5. Conclusions

This study presents a series of quasi-static tests to investigate the coupled axial tension-shear behavior of RC walls, and evaluates the influence of axial tensile forces on the cyclic shear performance of RC walls. The following conclusions can be drawn from this study:

(1) RC wall specimens showed three failure modes that were dependent on different values of axial tensile force. These modes were diagonal tension failure (no axial tensile force), shear-sliding failure

(normalized concrete tensile stress in the 0.51–1.43 range) and sliding failure (normalized concrete tensile stress in the 2.26–2.79 range).

(2) The shear strength of RC wall specimens decreased linearly with increasing axial tensile force, with a factor of approximately 0.35.

(3) Lateral stiffness value of the specimen subjected to very high tensile forces (n_c = 2.79) was approximately 20% of the stiffness values of the specimen having no axial load. Value of sliding shear strength in the former was 24% of the shear strength capacity of the specimen having no axial load.

(4) The ACI 318-14 (U.S.) code formulae provided a conservative estimate of the shear strength capacity of the RC wall specimens under axial tensile forces, with an average experimental-to-calculated ratio of 1.68. The JGJ 3-2010 (China) code formulae tended to overestimate the shear strength capacity of RC walls subjected to moderate axial tensile forces, with an average experimental-to-calculated ratio of 0.93.

Acknowledgements

This study was sponsored by the Scientific Research Fund of Institute of Engineering Mechanics, China Earthquake Administration (Grant No. 2017D08) and National Natural Science Foundation of China (Grant No. 51678347). The writers wish to express their sincere gratitude to the sponsors.

References

[1] Kato H, Tajiri S (2010): Preliminary reconnaissance report of the Chile earthquake 2010. Building Research Institute, Japan.

[2] Paulay T, Santhakumar AR (1976): Ductile behavior of coupled shear walls. *ASCE Journal of the Structural Division*, **102** (1), 93–108.

[3] Aktan AE, Bertero VV (1984): Seismic response of R/C frame-wall structures. *Journal of Structural Engineering, ASCE*, **110** (8), 1803–21.

[4] Xu P, Xue Y, Xiao C, Wang C, Sun H, Xu Z, Gu R (2005): Experimental study on seismic performance of high-rise SRC hybrid structures. *Building Structure*, **35** (5), 3-8 [in Chinese].

[5] Lehman DE, Turgeon JA, Birely AC, Hart CR, Marley KP, Kuchma DA, Lowes LN (2013): Seismic behavior of a modern concrete coupled wall. *Journal of Structural Engineering, ASCE*, **139**(8), 1371–81.

[6] Wang T, Lai T, Zhao H, Lin H, Wang Y (2017): Tensile-shear mechanical performance test of reinforced concrete shear wall. *Building Structure*, **47** (2), 64-69 [in Chinese].

[7] Cheng X, Ji X, Henry RS, Xu M (2019): Coupled axial tension-flexure behavior of slender reinforced concrete walls. *Engineering Structures*, **188**, 261-276.

[8] CMC (2010a): *Technical Specification for Concrete Structures of Tall Building (JGJ 3-2010)*. Beijing: China Ministry of Construction [in Chinese].

[9] CMC (2010b): *Code for Design of Concrete Structures (GB50010-2010)*. Beijing: China Ministry of Construction; [in Chinese].

[10] CMC (2015). *Specification of Testing Methods for Earthquake Resistant Building (JGJ 101-2015)*. Beijing: China Ministry of Construction. [in Chinese]

[11] ASCE (2014). *Seismic Rehabilitation of Existing Buildings. ASCE/SEI 41-13*. Reston, VA: American Society of Civil Engineers.

[12] Moehle J (2014): *Seismic Design of Reinforced Concrete Buildings*. New York: McGraw-Hill Education.

[13] ACI 318 Committee (2014): *Building Code Requirements for Structural Concrete (ACI 318-14) and Commentary*. Farmington Hills (MI): American Concrete Institute.

